Beam Energy Resolution of a Prototype BPM-based Energy Spectrometer for the International Linear Collider

R. Arnold [1], S. Boogert[2], V. Duginov[3], M. Hildreth[4], Yu.G. Kolomenski[5], A. Lyapin[6], S. Kostromin[3], ... , D. J. Miller[6], N. Morozov[3], H.J. Schreiber[7], ... , E. Torrence[8], M. Viti[6] and M. Woods[1]

[1] Stanford Linear Accelerator Centre, Menlo Park, CA, USA

[2] Royal Holloway, University of London, Egham , UK

[3] Joint Institute of Nuclear Resaerch, Dubna, Moscow Region, Russia

[4] University of Notre Dame, Notre Dame, IN, USA

[5] University of California and Lawrence Berkeley National Laboratory, Berkeley, CA, USA

[6] University of College London, England, UK

[7] Deutsches Elektronen-Synchrotron DESY, Hamburg and Zeuthen, Germany

[8] University of Oregon, Eugene, USA

Abstract

...
...
...

1 Introduction

The physics potential of the International Linear Collider (ILC) depends greatly on precise energymeasurements of the electron and positron beams at the interaction point (IP). Such measurements are mandatory in order to determine particle masses in high-rate processes. For example, measuring the top mass from a threshold scan to order of 100 MeV or measuring the Standard Model Higgs in direct reconstruction to about 50 MeV require knowledge of the luminosity-weighted mean collison energy $\sqrt{s}$ to a level of $1-2\cdot 10^{-4}$ to avoid center-of-mass energy uncertainties from dominating the experimental results. Precise incoming beam energy (E_b) measurements are a critical component to $\sqrt{s}$ determination as it sets the overall energy scale for the collision process.

The strategy proposed in the ILC design [1] is to have redundant beam-based measurements capable to achieve a 10^{-4} relative precision on a single beam, which would be available in real time as a diagnostic tool to the operators. Also, physics reference channels such as $e^+e^- \rightarrow \mu^+\mu^-\gamma$ where the muons are resonant with the known Z-mass are expected to provide valuable cross-checks of the collison scale, but only long after the data have been recorded.

The primary method planned to perform E_b measurements is a non-evasive beam position monitor based spectrometer as initially proposed in [2], located upstream of the interaction point just after the energy collimators of the beam delivery system (BDS). The baseline ILC spectrometer design uses two dipole magnets to produce a beam displacement x, while two more magnets return the beam to the nominal beam orbit. For such a chicane, the beam energy is then given by

$$E_b = \frac{c \cdot e \cdot L}{x} \int\limits_{magnet} Bdl \quad , \tag{1}$$

where L is the distance between the magnets and $\int Bdl$ the B-field integral in each magnet. A 4-magnet chicane avoids spurious beam displacement signals in the BPMs due to beam tilts, and thus systematic errors in E_b measurements. For this reason, a 4-magnet spectrometer, which maintains the beam axially with respect to the axis of the cavity BPMs, is preferable over a more conventional 3-magnet chicane [2, 3]. Furthermore, in a 4-magnet chicane the B-field can be varied from $-B_{max}$ to $+B_{max}$ to study systematic effects, without changing beam orientation.

The BPM-based chicane is modeled after the spectrometer for LEP-II [3] used to callibrate the energy scala for the W-mass measurement. At the

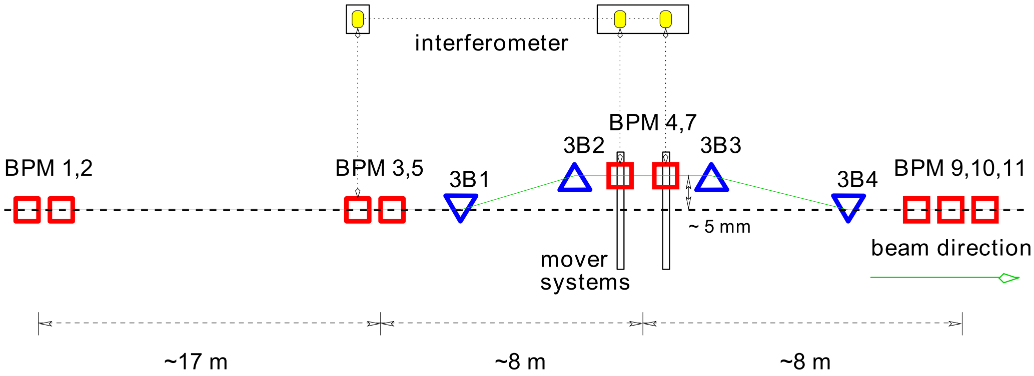

Figure 1: Schematic representation of the magnetic chicane in ESA. Main diagnostics instruments also are shown.

ILC, however, the parameters of the spectrometer are tighty constraint to provide limited emittance dilution at the highest ILC energy of 500 GeV.

When operating the spectrometer with a fixed dispersion of $\sim$5 mm at the center over the whole energy range, a BPM resolution of 0.5 μm is needed. Such a precision (or better) can be achieved with cavity beam position monitors [4]. Since the spectometer bending magnets are needed to operate at low magnetic field when running at the Z-pole the B-field measurement may not be accurate enough. But significantly improved BPM resolution would allow to run the dipoles at the same field for both the Z-pole and highest energy operation.

Absolute energy measurement requires that the beam orbit with no field is measured. There is an ongoing R&D program to determine how to perform accurate field mesurements for low fields, or even zero fields.

A protype test setup for a 4-magnet spectrometer was commissioned in 2006 (the T-474 experiment) and extented in 2007 (the T-491 experiment) in the End Station A beamline at SLAC [5]. The setup involes four dipoles and some BPMs, as schematically shown in Fig. 1, and high-precison RF BPMs in front, behind and in between the magnets.

The electron beam generated by the main Linear Accelerator at SLAC was transported into the A-line on its way to ESA. The ESA beam operates with single bunches at 10 Hz and a nominal energy of $E_b = 28.5$ GeV, a bunch charge of $1.6 \cdot 10^{10}$ electrons, a bunch length of $\sim$500 μm and an energy spread of 0.15%, i.e. with properties similar to ILC expectaions. These properties make the ESA test beam a unique enviroment for testing the capabilities of

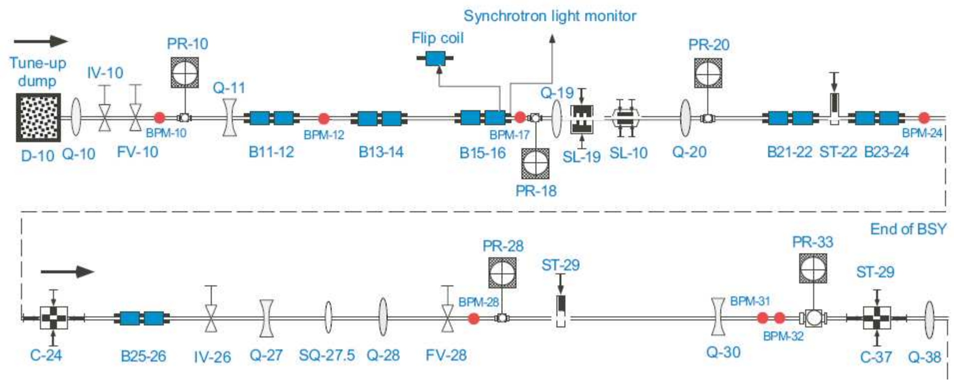

Figure 2: The beam line configuration for the A-line up to the ESA experimantal hall. The beam goes from left to right, top to bottom.

the proposed spectrometer.

The paper is organised as follows. Sect. 2 describes the hardware configuration of the final ESA test setup. Sect. 3 ...

2 Test Beam Setup Hardware Configuration

The T-474/491 experiment is housted at the End Staion A at the Stanford Linaer Accelerated Centre, USA. The beam used is generated by the the main Lineac and accelerated to the energy of 28.5 GeV. At the end of the acceleration tunnel the beam was transported from the Beam Switchard Yard through large bending magnets into the A-line on its way to ESA. The A-line of about 300 m length involves dipoles and quadrupoles to bend, respectively, to control the transverse beam size, and diagnostic instruments such as stripline and RF cavity BPMs, charge sensitive toroids, a synchrotron light monitor, profile screens and diodes. A control program feed back-system stabilizes the beam position at the end of the A-line. The maximun momentum acceptance amounts to 2%. Details on the beam line are sketched in Fig. 2. ??? Where are BPM 12 and 24 ??? I think a better figure exists in the BPM paper of Slater et al. The beam posion monitors BPM 12 and BPM 24 at hig dispersion points of ??? mm, respectively, ??? mm are used to estimate the A-line energy resolution (see. Sect. ???), so that cross-checks against the ESA spectrometer measurement are possible.

Name and Type of the device	Field component	Working range
NMR 3B1A		0.043 - 0.13 T
NMR 3B1B		0.09 - 0.26 T
NMR 3B2C		0.09 - 0.26 T
NMR 3B3D		0.09 - 0.26 T
NMR 3B4E		0.09 - 0.26 T
Hall probe	Y Component	
Fluxgate 1	Y/X Component	
Fluxgate 2	Y Component	

Table 1: Types of probes used for the magnetic chicane in ESA.

The final ESA spectrometer (Fig. 1) consists of four bending magnets denotes as 3B1, 3B2, 3B3 and 3B4 and a number of BPM doublets and triplets. The magnets 10D37 from the old SPEAR injection beam line were only slighly refurbished before their installation into ESA. They bend the beam horizontally or in X-direction. The magnets are 37" in length with 10"-wide pole faces. The vertical gap is 3". They are run in series from a single power supply. The magnets were studied during a set of measurements in the Magnet Measurement Laboratory at SLAC. Their stability, reproducibility and constency were determined. Magnetic field maps of the vertical field component B_y were also taken using NMR and Hall probes, while each $\int Bdl$ was measured using a flip coil, which was calibrated against a moving wire system. Details of the field measurements can be found in [6, 7, 8].

In situ at ESA, two NMR probes and one Hall probe were installed in the first magnet 3B1, while one NMR probe was postioned in each other three magnets, so that magnetic field integral values could be monitored. In the test data runs, the nominal B-field was 0.117 Tesla·m which corresponds to a magnet operation with 150 A. The stray field outside the magnets in the middle of the chicane was monitored using two low-field-fluxgate magnetometers. One was placed on the girder to obtain x- and y-field components and the other on the beam pipe for only the y-component. Properties of the probes and fluxgate monitors are summarized in Tab. 1.

In an extented version of the ESA spectrometer an additional device was installed, the synchrotron radiation (SR) energy spectrometer [9]. It consists of a wiggler in between 3B3 and 3B4 (not shown in Fig. 1) and SR detectors, in analogy to the WISRD experiment performed at SLAC [10] some years ago. The Hall probe of magnet 3B1 was now moved to the wiggler magnet.

Such a spectrometer has been also proposed for the ILC to deduce beam energy information after the e^+e^- collision point.

In order to measure the beam orbit, 8 BPMs were installed: three types of S-band cavity BPMs (BPM 3, 4, 5) and 5 SLAC A-line and linac type BPMs (BPM 1,2, 9, 10, and 11) (???). BPM 7 was designed and manufactured by UCL and aimed of a prototype for the BPM-energy spectrometer at the ILC. The ILC prototype monitor is a cylindrical cavity with wave guide coupling system providing signals for both X and Y and suppressing unwanted modes. The SLAC BPMs consists of 2 rectangular cavities, one for X- and one for Y-direction, and a cylindrical cavity to provide the phase and charge information.

BPM 4 (and BPM 7) in the center of the chicane was instrumented with an X-Y mover system which provides exact X-position and precise calibration of this BPM. The mover system was also used for tracking the beam while the magnets were operated. A high precision interferometer system monitored the horizontal motion of BPMs 3, 4 and 5 (???). The performance of the BPM system is discussed in [4]. The upstream BPMs 1, 2, 3 and 5 define a beam orbit from a fit to the location of BMP 4 for runs with no magnetic fields, and so a reference position of the beam at BPM 4 exists.

3 Energy Resolution

3.1 A-line Energy Resolution

Before discussing E_b measurements from the BPM spectrometer we present beam energy measurements from the A-line diagnostic BPMs at high dispersion points, about 40 m (???) upstream of ESA. ...

M.V. original text:

During 2007 a complete 4-magnet chicane was commissioned in ESA so that beam energy measurements could be performed[**?**, **?**]. Here only some general arguments are discussed which are needed to evaluate the resolution of the measurements. The structure of this note is as follows. In Sect. 4 an overview of the 4-magnet chicane is given. In Sect. 5 the BPMs within the SLAC A-line (the energy BPMs) will be described including their resolution. Section 6 evaluates the beam energy resolution of the 4-magnet chicane and compares the results with those from the energy BPMs. The last section, Sect. 7, contains the conclusions.

The data from the experiment T474 were collected in “runs”, where a run had a duration of typically $10 \div 20$ minutes. The data were handled by a Labview program running on a Windows XP computer and, after some reorganization, the measurements were stored into root files.

For a given run, the field of the magnets was kept fixed and only changed periodically for positive polarity, zero current and negative polarity runs. Over the 3-weeks data taking period, several operation modes such as energy scans and calibration procedures were performed. Calibration runs also collected data from the corrector dipoles, Helmholtz coils and mover systems.

Energy scans were performed by changing the beam energy from the nominal value $E_b = 28.5$ GeV in 5 steps of 50 MeV between $E_b \pm 0.1$ GeV, i.e. over a 200 MeV total energy range. In the following sections only these data will be discussed.

4 The 4-Magnet Chicane in End Station A

Figure 3 shows a schematic view of the 4-magnet chicane in ESA. The magnets were installed on a girder, using supports made of non-ferromagnetic material. Only one power supply was available for the magnets mounted in series, so that the current was the same for all of them. By means of a Linux computer it was possible to set the nominal values of the B-field integral. The nominal values were converted into a current by the control program, using a linear relation[**?**]. In Fig. 3 also some details on diagnostics of the spectrometer are visible. Magnet 3B1 was equipped with two NMR probes and one Hall probe, whereas the other magnets had only one NMR probe. The standard current used was ± 150 A, which corresponds to a B-field of ± 0.11 T and a 5 mm dispersion in the center of the chicane (mid-chicane) for an electron beam of 28.5 GeV. The two NMR probes in 3B1 were of different types with different working ranges. They, however, overlapped in the region of the B-field setting. The Hall probe, placed in magnet 3B1 only for runs in March 2007, was removed after that to be installed in the wiggler magnet for experiment T475.

Along the beam line, two flux gate monitors were also placed in the mid-chicane to provide access to the stray field. One was placed on the girder to read the X- and Y-field components and the other on the beam pipe reading only the Y-component.

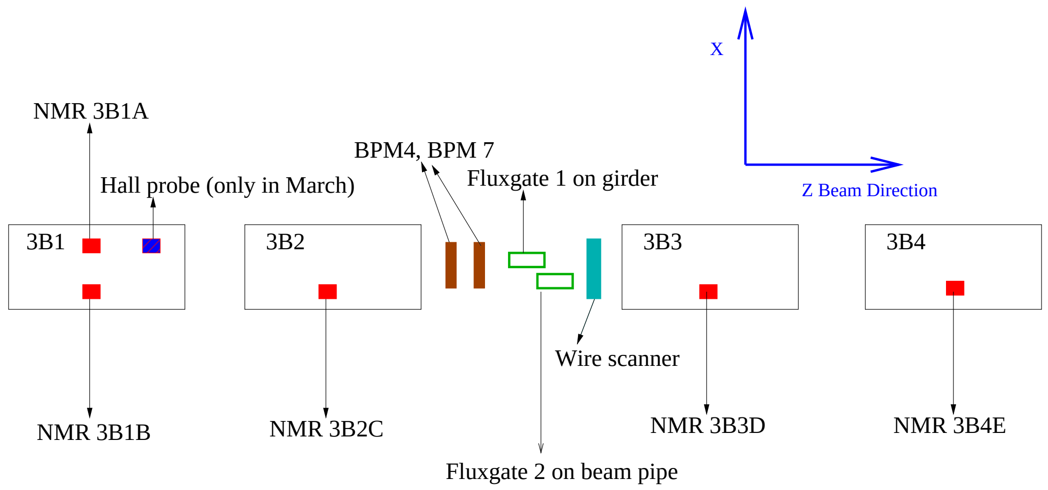

Figure 3: Schematic representation of the magnetic chicane in ESA. Also the main diagnostics instruments are shown.

5 Energy BPMs

Within the bend in the A-line, some BPMs were installed to provide the relative variation of E_b, the nominal beam energy, through their X-position readings. The data available were the X-position and the tilt in the XZ-plane of BPMs 12 and 24. In the following, these variables are denoted as x24Pos, x12Pos, x24Tilt and x12Tilt. At the locations of the BPMs in the A-line, the X-positions and the tilts θ of the beam are related to the beam energy through $E_b \propto 1/x \propto 1/\theta$, neglecting possible position jitters of the beam. Thus, the relative energy resolution σ_{E_b}/E_b can be estimated as

$$\frac{\sigma_{E_b}}{E_b} = \frac{\sigma_{\mathrm{x}}}{\mathrm{x}} , \tag{2}$$

where x represents one of the variables x24Pos, x12Pos, x24Tilt and x12Tilt.

In a first step, all quantities used were normalized in order to be able to compare them to each other. Denoting x as a generic raw variable, the normalized quantity x' is defined as

$$x' = \frac{x - \bar{x}}{\Delta_x} , \tag{3}$$

where $\bar{x}$ is the mean value of the variable x in question and Δ_x the standard deviation calculated for a given number of events.

In Figs. 4 and 5 position measurements of BPM 12 and 24 are shown from an energy scan performed for a run with the magnet current set to +150 A. Each point corresponds to a beam bunch of 10^{10} particles and as seen on the figures, for a fixed energy a cluster of points exists which is mainly due to the beam energy jitter. The five energy steps of the scan at E_b-100 MeV, E_b-50 MeV, E_b, E_b+50 MeV, E_b+100 MeV are clearly visible.

In Fig. 4 the concept of the normalization procedure is addressed for the raw X-position data of BPM 12, shown left. Since the BPM values shown are not calibrated, the Y-axis is given in arbitrary units. The histogram on the right-hand side is the projection of the data of Fig. 4 (left) to the Y-axis, from which the mean value $\bar{x}$ and the RMS Δ_x can be deduced. It is important to note that Δ_x and the resolution σ_{X} in Eq. (2) are different quantities. The first quantity represents the width of the data used for normalization, while the latter one denotes the error on position or tilt measurements.

An example of the normalization is presented in Fig. 5, where for an energy scan the raw X-position readings of BPM 12 and 24 (left) and the normalized data (right) are shown. The raw x24Pos measurements have different mean values and standard deviation than those of BPM 12, but after normalization, both data sets superimpose almost perfectly. In plots of normalized data, the Y-axis will be always given in "a.u.", i.e. in arbitrary units. .

The two dashed lines on the right-hand side of Fig. 5 indicate the total range in energy where the scan was performed. This range of about 3 for the normalized case corresponds to 200 MeV in terms of beam energy. This correspondence of 3 to 200 MeV provides the scale factor of the energy resolution procedure.

5.1 Energy BPM Resolution

Considering the normalized variables x24Pos, x12Pos, x24Tilt, x12Tilt as independent, it is possible to estimate their resolutions by means of the histograms in Fig. 6. Each histogram represents, for a given energy scan, the difference between two out of the four variables, bunch-to-bunch. Not all possible combinations are shown. It is important to note that the difference between two quantities with different dimensions, like position and tilt, is now after normalization physically meaningful.

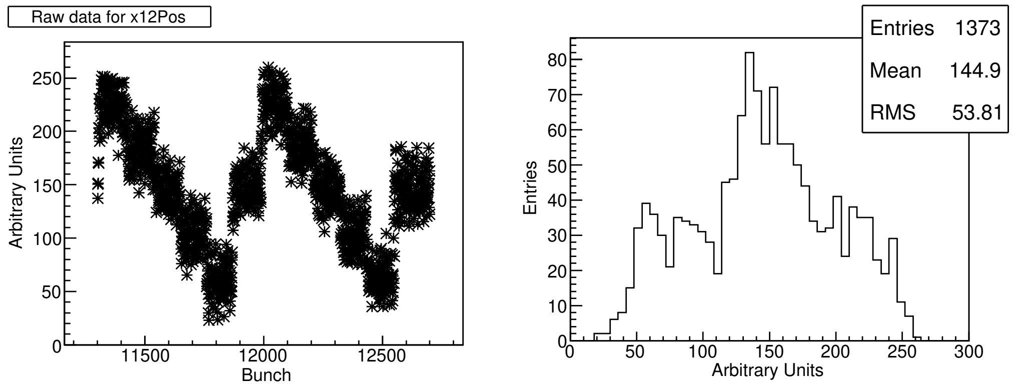

Figure 4: Left: Raw X-position readings for BPM 12 for an energy scan. Right: Projection of the data of the left-hand side to the Y-axis.

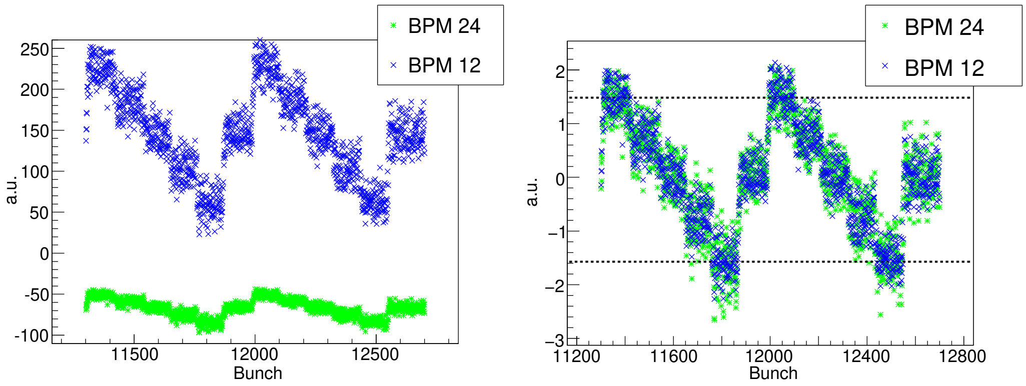

Figure 5: Left: Raw variables x12Pos and x24Pos for an energy scan. Right: Position data of the left-hand side after normalization. The two dashed lines indicate the scan range used.

From Fig. 6 one derives

$$\left\{ \begin{array}{lllll} \sigma_1^2 & = & \sigma_{x24Pos}^2 + \sigma_{x12Pos}^2 & = & (0.1865)^2 \\ \sigma_2^2 & = & \sigma_{x24Pos}^2 + \sigma_{x12Tilt}^2 & = & (0.2151)^2 \\ \sigma_3^2 & = & \sigma_{x12Pos}^2 + \sigma_{x24Tilt}^2 & = & (0.1231)^2 \\ \sigma_4^2 & = & \sigma_{x12Pos}^2 + \sigma_{x12Tilt}^2 & = & (0.125)^2 \ , \end{array} \right. \tag{4}$$

while, if the measurements are independent and possible position jitters are neglected, all σ's should be zero for an ideal situation. Any non-zero value indicates a finite resolution of the BPM. Solving the system (4) for σ_{x24Pos},

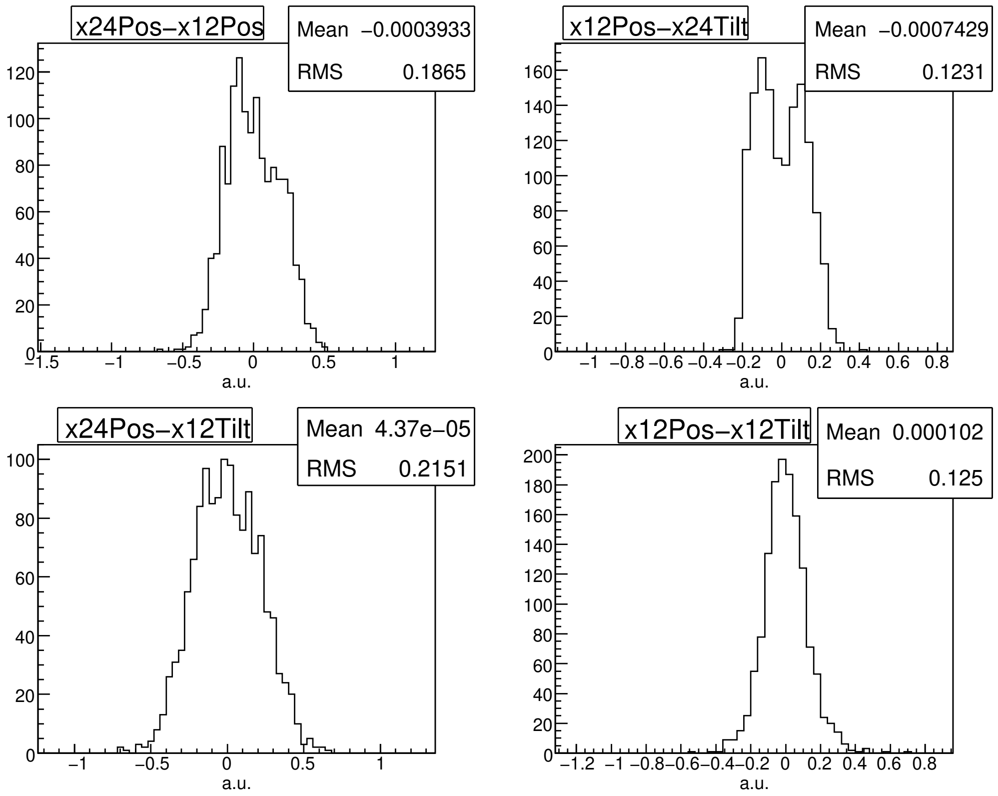

Figure 6: Differences between the variables as indicated for an energy scan.

σ_{x12Pos}, $\sigma_{x24Tilt}$ and $\sigma_{x12Tilt}$, we obtain

$$\begin{cases} \sigma^{a.u.}_{x24Pos} & = & 0.187 \\ \sigma^{a.u.}_{x12Pos} & = & 0.018 \\ \sigma^{a.u.}_{x24Tilt} & = & 0.12 \\ \sigma^{a.u.}_{x12Tilt} & = & 0.124 \; , \end{cases} \tag{5}$$

where $\sigma^{a.u.}$ means that the quantity in question is expressed in arbitrary units of the normalized scale. According to Eqs. (2) and (3), we obtain

$$\frac{\sigma^{a.u.}}{3} = \frac{\sigma^{MeV}}{200} \; , \tag{6}$$

so σ^{MeV}_{x12Pos}, defined as the resolution of the variable x12Pos for a relative beam energy measurement, can be written as $\sigma^{MeV}_{x12Pos} = 0.018 \cdot 200/3 = 1.2$ MeV, which corresponds to

$$\frac{\sigma^{MeV}_{x12Pos}}{E_b} = \frac{1.2 \text{ MeV}}{28.5 \text{ GeV}} = 4.2 \cdot 10^{-5} \; . \tag{7}$$

The other variables like x24Pos provide worse beam energy resolutions, up to an order of magnitude.

It is worthwhile to remind that the energy BPMs do not provide an absolute but only a relative beam energy measurement, i.e. no determination of E_b is possible.

6 ESA Magnetic Chicane

The basic scheme of the spectrometer in End Station A was shown in Fig. 3. Unfortunately, in the 2007 March runs the readout of the NMR probes was not working properly and in July the two NMR probes installed in magnet 3B1 and the one in 3B3 were damaged. Thus, essential informations for absolute beam energy measurements were missing. Moreover, since a complementary or independent method for E_b measurement was a priori not foreseen in ESA, the results from the chicane could not be cross-checked or cross-calibrated. Only relative beam energy measurements could be performed.

6.1 Mid-chicane BPM 4

For the following analysis only data from the July 2007 runs are taken into account and, if not explicitly stated, all variables considered are unnormalized. Since BPM 7, also positioned in the mid-chicane, was not reliable, only data from BPM 4 will be employed.

Selecting the energy scan data from run 2743 as an example, Fig. 7 shows the X-reading of BPM 4 (x4Pos). Here, steps in energy cannot be recognized, unlike to Fig. 5, since position fluctuations of the beam are bigger than the energy steps applied.

In fact, referring to Fig. 8, the dispersion d can be written as

$$\mathrm{d} = x^{(4)}_{chicane}(E_b) = \mathrm{x4Pos} + A - x^{(4)}_{jitter} \ , \tag{8}$$

where $x^{(4)}_{chicane}(E_b)$ is the beam offset in the mid-chicane at the BPM 4 beam line position, which is coupled to the beam energy through the relation $X \propto 1/E_b$, $x^{(4)}_{jitter}$ the extrapolation position of the beam at the same Z-position (see Fig. 8) and A the BPM offset, which ensures to locate the beam close to the center of the BPM. The value of A varies with the B-field, for example, when switching the magnet polarity or when running with zero-magnet current. Nevertheless, since we normalize the data at the end of the analysis, this offset is not important and allows us to write

$$\mathrm{x4Pos} = x^{(4)}_{chicane}(E_b) + x^{(4)}_{jitter} \ . \tag{9}$$

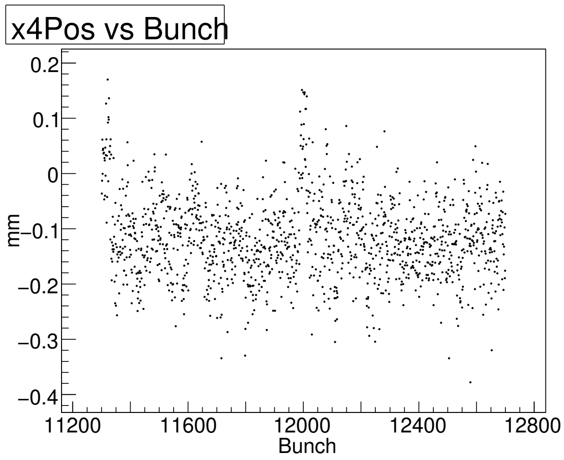

Figure 7: Beam positions of BPM 4 (without normalization) of an energy scan.

In order to have access to the offset $x^{(4)}_{chicane}(E_b)$ it is necessary to subtract $x^{(4)}_{jitter}$ from x4Pos. $x^{(4)}_{jitter}$ can be deduced from an extrapolation of the beam using position values from BPMs 1,2,3,5,9,10,11 (see [?]) . It is obvious that for zero-current runs $x^{(4)}_{chicane}(E_b) = 0$ and, hence, x4Pos=$x^{(4)}_{jitter}$.

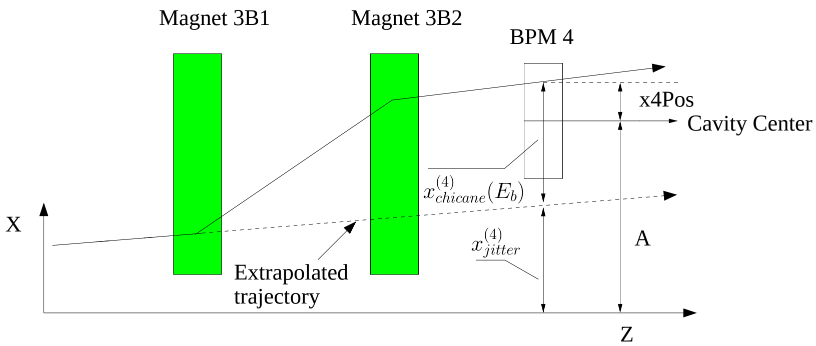

Figure 8: Working principle of the chicane: a charged particle traveling through the spectrometer receives an additional offset inversely proportional to its energy. The X-position reading of BPM 4 is the sum of two quantities, the extrapolated position $x^{(4)}_{jitter}$ and the offset $x^{(4)}_{chicane}(E_b)$.

6.2 Evaluation of $x^{(4)}_{jitter}$

The simplest way to determine $x^{(4)}_{jitter}$ is to perform a linear fit through the BPM beam position values upstream and downstream of the chicane and to extrapolate the straight line to the Z-position of BPM 4. This method is, however, limited since it does not take into account any coupling between X- and Y-positions of the BPMs and other informations as the tilt. Rotation or misalignment informations of the BPMs are missing and could therefore not be implement into the analysis. Also, the offsets of the centers of the BPMs should be known, whose determination is also a non-trivial task.

Figure 9 shows $x^{(4)}_{jitter}$ as inferred from BPMs 1,2,3,5 upstream of the chicane against the BPM 4 X-position readings. The data are from a run, where the magnet current was set to zero, so that x4Pos $= x^{(4)}_{jitter}$. The dashed line in Fig. 9 represents a straight line with a slope of 1. It is evident that x4Pos $= \alpha \cdot x^{(4)}_{jitter}$, with $\alpha \neq 1$, which might be caused by e.g. different offset or rotations of the BPMs around the Z-axis. In general, x4Pos can be written as

$$\text{x4Pos} = \alpha \cdot x^{(4)}_{jitter} + \beta \cdot x^{(4)}_{chicane}(E_b) \ , \tag{10}$$

where β denotes a possible relative rotation of BPM 4 with respect to the dipole field.

Thus, a more appropriate approach seems to be necessary to predict the correct value of $x^{(4)}_{jitter}$, with $\alpha = 1$ (a discussion on β will be presented

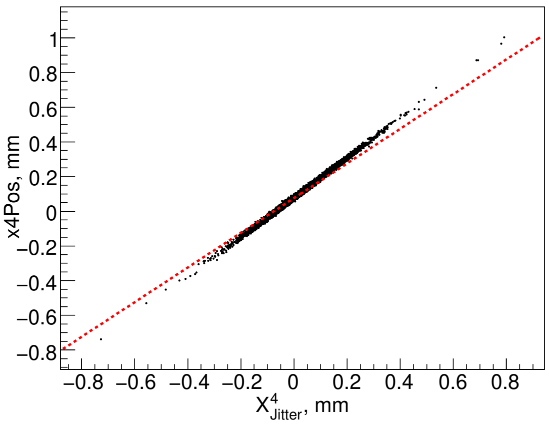

Figure 9: BPM 4 position measurement vs. $x^{(4)}_{jitter}$ evaluated from a linear extrapolation of the X-positions from BPMs 1,2,3,5.

later, but for the moment we assume $\beta = 1$). One option for an improved $x^{(4)}_{jitter}$ evaluation relies on the assumption that $x^{(4)}_{jitter}$ depends linearly on other BPM variables upstream and/or downstream of the chicane. Figure 10 shows, as an example, x4Pos plotted against x5Pos (left) and x5Tilt (right) from BPM 5. The data are not normalized and were taken from a run with zero-current (run 2747). A clear correlation between the variables exists in both cases. The beam jitter at BPM 4 can therefore be written as

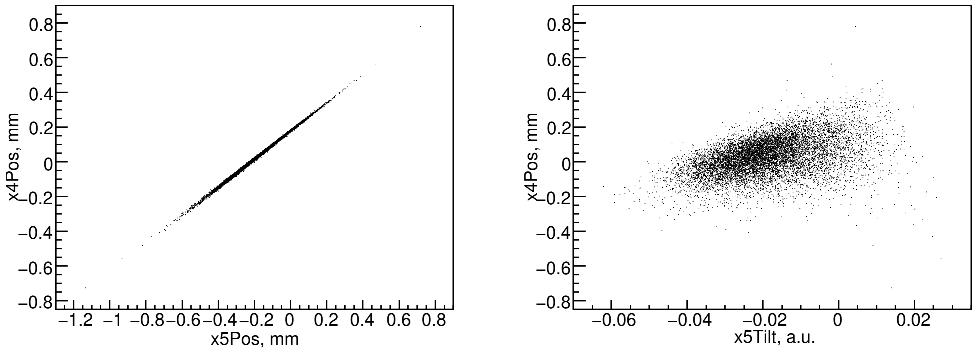

Figure 10: x4Pos as a function of x5Pos (left) and x5Tilt (right) for a run with zero-current.

$$
\begin{aligned}
x^{(4)}_{jitter} \quad = \quad & c^0 + c^1_1 \cdot \mathrm{x1Pos} + c^2_1 \cdot \mathrm{x1Tilt} + c^3_1 \cdot \mathrm{y1Pos} + c^4_1 \cdot \mathrm{y1Tilt} \\
& \vdots \\
& + c^1_j \cdot \mathrm{xjPos} + c^2_j \cdot \mathrm{xjTilt} + c^3_j \cdot \mathrm{yjPos} + c^4_j \cdot \mathrm{yjTilt} \\
& \vdots \\
& + c^1_N \cdot \mathrm{xNPos} + c^2_N \cdot \mathrm{xNTilt} + c^3_N \cdot \mathrm{yNPos} + c^4_N \cdot \mathrm{yNTilt} \ ,
\end{aligned}
\tag{11}
$$

where xjPos and yjPos denote the X-, respectively, Y-position, xjTilt and yjTilt the corresponding tilts of the j-th BPM and N the total number of BPMs used. For a run with magnet current set to zero, the coefficients c^j_i are determined by minimizing the quantity

$$
\sum_{i=1}^{N_{event}} (\mathrm{x4Pos} - x^{(4)}_{jitter})^2_i \ . \tag{12}
$$

The results for the coefficients c^j_i so obtained are discussed in Sect. 6.4.

6.3 Dipole Magnets

An essential prerequisite of the spectrometer is that the beam position downstream of the chicane is not coupled with that within the chicane, which means that the upstream beam path must be restored downstream. In other words, the chicane has to act on the beam in a symmetric manner. B-field measurements were performed in March 2007 to study the response of the chicane. Some results are shown in Fig. 11. Here, differences between the measured and nominal B-fields are plotted as a function of the nominal value, for negative and positive polarities.

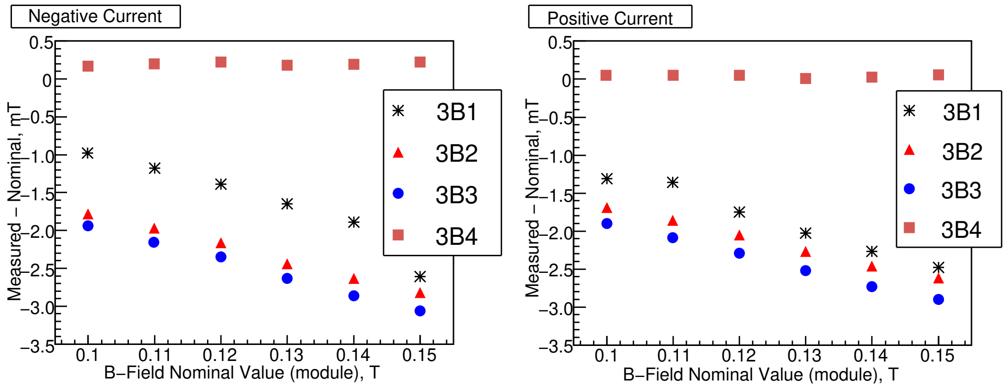

Figure 11: Differences between the measured and nominal B-fields as a function of the nominal value of the four magnets in ESA. Left: Negative current. Right: Positive current.

For magnet 3B1, only the Hall probe was employed, whereas for the other magnets NMR probes were used. As can be seen, the differences vary from few tenths of mT (for magnets 3B2 and 3B3) up to about 3 mT. Magnet 3B4 shows field values much closer to the nominal ones, because only for this magnet the relation between the current and the field as given in [?] was determined and used for the field settings. The differences seen in the Fig. 11 might be attributed to any residual field, which was estimated to be $0.2 \div 0.4$ mT (see [?]) and which is expected to depend on the history of the magnet and on the steel properties (no careful design and composition of the steel were accounted for). As a consequence, the path of the beam upstream could not fully restored downstream by the chicane, and changes of the beam energy are converted to position variations in BPMs 9, 10 and 11.

This supposition is supported by the following discussion. Similarly to what was done for BPM 4, the X-position of BPM 9 downstream of the chicane can be written as

$$\text{x9Pos} = x^{(9)}_{jitter} + x^{(9)}_{chicane}(E_b) \ . \tag{13}$$

For simplicity, α and β are assumed to be 1. If BPM 1, 2, 3 and 5 position data are used to predict the X-position jitter at BPM 9 ($x^{(9)}_{jitter}$) and if this value is subtracted from x9Pos for an energy scan, $x^{(9)}_{chicane}(E_b)$ as shown in Fig 12 is obtained. The steps due to different beam energies are basically visible which should however not be the case. Only position jitters with horizontal fluctuations around zero are expected. This observation supports that the BPMs downstream of the chicane are not useful to be used to estimate the beam jitter in BPM 4, $x^{(4)}_{jitter}$.

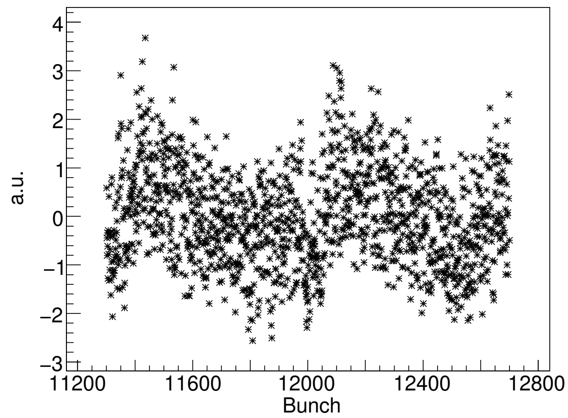

Figure 12: Normalized beam position of BPM 9 for an energy scan after subtraction of the jitter obtained from BPMs 1, 2, 3 and 5.

6.4 Energy Resolution of the Spectrometer

Using data from a particular zero-current run, the parameters c_i^j were determined by minimizing expression (12), described in Sect. 6.2, by accounting for X- and Y-position as well as X- and Y-tilt data from BPMs 1, 2, 3 and 5.[1]

Using the coefficients c_i^j obtained, $x^{(4)}_{jitter}$ can be calculated from Eq. (11) and if x4Pos is now plotted against the new $x^{(4)}_{jitter}$, a straight line with a

[1]If only X-position and X-tilt measurements are taken into account, less precise results are obtained, see also the discussions in Sect. 6.4.1.

slope close to 1 is obtained, see Fig. 13. This result demonstrates that $x^{(4)}_{jitter}$ after minimizing (12) is much more suitable than the procedure discussed at the beginning of Sect. 6.2.

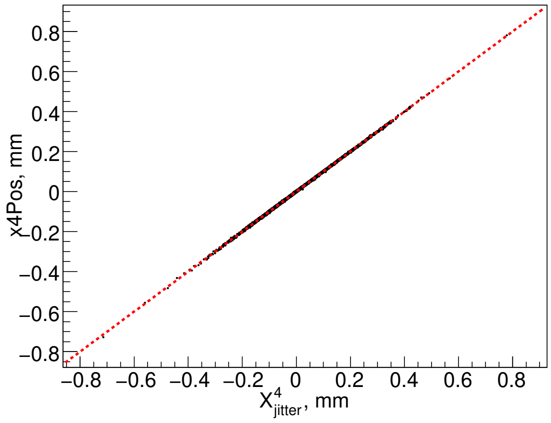

Figure 13: The position x4Pos versus $x^{(4)}_{jitter}$ evaluated using Eq. (11). The data are from a run with magnet current set to zero.

6.4.1 Beam Energy Resolution

The relative beam energy resolution of the 4-magnet chicane was performed in the following way. Considering an energy scan with magnet current of +150 A and enabling subtraction of $x^{(4)}_{jitter}$ from x4Pos, the beam offset in the mid-chicane, $x^{(4)}_{chicane}(E_b)$, is obtained from Eq. (9). In Fig. 14 (left) the normalized x12Pos and $x^{(4)}_{chicane}(E_b)$ data are superimposed, while on the right-hand side their difference (x12Pos - $x^{(4)}_{chicane}(E_b)$) is shown. The non-zero standard deviation of the histogram given in arbitrary units, $\sigma^{a.u.}$, is due to the finite resolution of $x^{(4)}_{chicane}(E_b)$ as well as of x12Pos. In fact,

$$\sigma^{a.u.} = \sigma^{a.u.}_{x^{(4)}_{chicane}(E_b)} \oplus \sigma^{a.u.}_{x12Pos} = 0.365 \ , \tag{14}$$

where the two terms were added in quadrature. $\sigma^{a.u.}_{x12Pos}$ was evaluated as 0.0187 in Sect. 5.1 and is negligible, so that

$$\sigma^{a.u.} \simeq \sigma^{a.u.}_{x^{(4)}_{chicane}(E_b)} \simeq 0.365 \ . \tag{15}$$

$\sigma^{a.u.}_{x^{(4)}_{chicane}(E_b)}$ can be understood as the normalized beam energy resolution of the 4-magnet chicane. Accounting for the correspondence between normal-

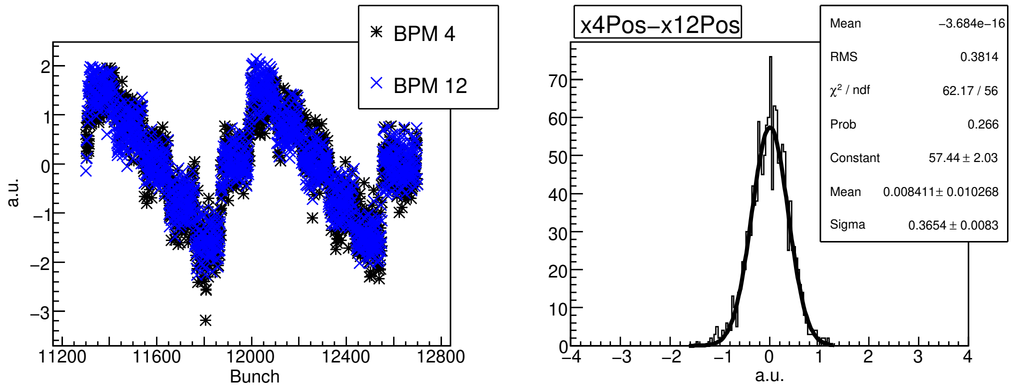

Figure 14: Left: Normalized position x4Pos after subtraction of the jitter and the position x12Pos, for an energy scan with magnet current of +150 A. Right: Difference between $x^{(4)}_{chicane}(E_b)$ and x12Pos.

ized and unnormalized variables, we conclude

$$\begin{aligned} \sigma^{MeV}_{x^{(4)}_{chicane}(E_b)} &= \sigma_{E_b} = 0.365 \cdot 200/3 = 24.3 \text{ MeV} \\ &\rightarrow \frac{\sigma_{E_b}}{E_b} = \frac{24.3 \text{ MeV}}{28.5 \text{ GeV}} = 8.5 \cdot 10^{-4} \; . \end{aligned} \tag{16}$$

If only the X-positions and X-tilts of BPMs 1, 2, 3 and 5 are taken into account, $x^{(4)}_{jitter}$ is less precise and the energy resolution becomes $\sigma_{E_b}/E_b \simeq 8.9 \cdot 10^{-4}$. This value is close to that in Eq. (16), which means that the variables yPos and yTilt have no strong impact on $x^{(4)}_{jitter}$ and, hence, on the energy resolution.

In principle, σ_{E_b}/E_b can be estimated in a complementary way. Since $x^{(4)}_{chicane}(E_b) =$ x4Pos - $x^{(4)}_{jitter}$, the resolution of $x^{(4)}_{chicane}(E_b)$ is equivalent to the resolution of the difference (x4Pos - $x^{(4)}_{jitter}$). Figure 15 shows this difference for a run with zero magnet current. For this case, (x4Pos - $x^{(4)}_{jitter}$) is expected to be zero for every bunch, but the resulting standard deviation is non-zero. Interpreting this non-zero value as the resolution of (x4Pos - $x^{(4)}_{jitter}$), respectively, $x^{(4)}_{chicane}(E_b)$ and accounting for the dispersion $x^{(4)}_{chicane}(E_b) \simeq 5$ mm in the mid-chicane, Eq. (2) becomes

$$\frac{\sigma_{x^{(4)}_{chicane}(E_b)}}{x^{(4)}_{chicane}(E_b)} = \frac{\sigma_{E_b}}{E_b} = \frac{2.3 \ \mu\text{m}}{5 \text{ mm}} = 4.6 \cdot 10^{-4} \; . \tag{17}$$

This result is considerably better than that in (16). Possible reasons for the difference might be some non-demagnetization after switching off the

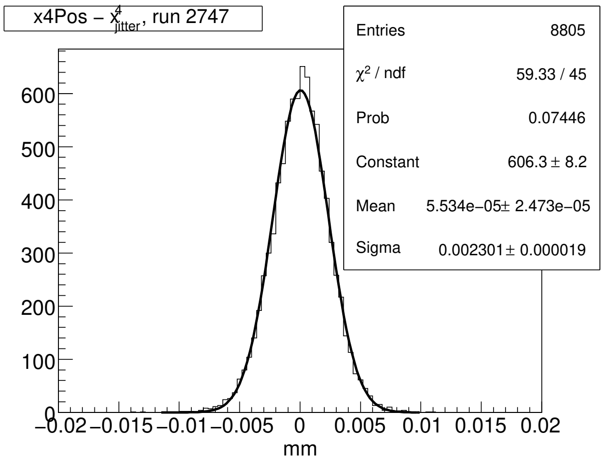

Figure 15: Difference between x4Pos and $x^{(4)}_{jitter}$ for a zero-current run. $x^{(4)}_{jitter}$ is calculated using the parameters from the minimization procedure as described in Sect.6.2.

magnets and/or a non-equal to 1 value of β in Eq. (10). In fact, if a rotation of BPM 4 with respect to the dipole field by an angle θ exists, the effective offset at the mid-chicane is 5 mm $\cdot \cos\theta$ and the error on the relative beam energy measurement becomes

$$\frac{\sigma_{E_b}}{E_b} = \frac{2.3\ \mu\mathrm{m}}{5\ \mathrm{mm} \cdot \cos\theta} > 4.6 \cdot 10^{-4}\ , \tag{18}$$

which points into the right direction.

6.5 X- and Y-Position Coupling

In analogy to X-jitter determination, it is possible to estimate the jitter in Y-direction, $y^{(4)}_{jitter}$, and, after subtraction from y4Pos, $y^{(4)}_{chicane}(E_b)$ can be deduced. In Fig. 16, $y^{(4)}_{chicane}(E_b)$ is plotted against $x^{(4)}_{chicane}(E_b)$ for an energy scan. Some correlation between X- and Y-positions is clearly visible, which reveals that β in Eq. (10) is definitely different from 1. This can be caused by a rotation of BPM 4 relative to the magnetic field as already stated in the previous section. Thus, to improve the relative beam energy resolution, also $y^{(4)}_{chicane}(E_b)$ should be taken into account in the analysis.

One way to include $y^{(4)}_{chicane}(E_b)$ is to perform a rotation in the (X,Y)-plane. After jitter subtraction, two new variables are defined as

$$\begin{pmatrix} (x^{(4)}_{chicane}(E_b))_{rot} \\ (y^{(4)}_{chicane}(E_b))_{rot} \end{pmatrix} = \begin{pmatrix} \cos\theta & -\sin\theta \\ \sin\theta & \cos\theta \end{pmatrix} \begin{pmatrix} x^{(4)}_{chicane}(E_b) \\ y^{(4)}_{chicane}(E_b) \end{pmatrix} . \tag{19}$$

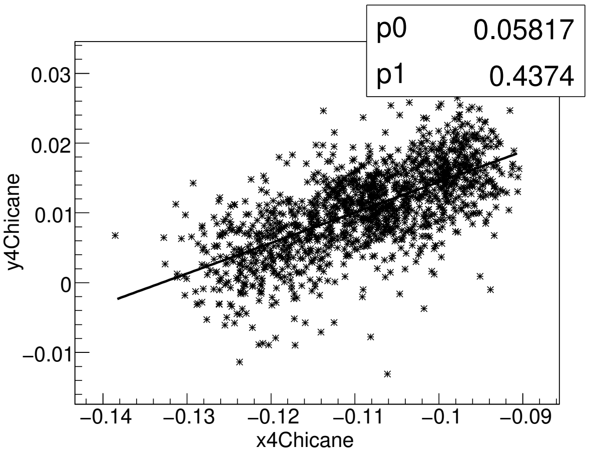

Figure 16: $y^{(4)}_{chicane}(E_b)$ versus $x^{(4)}_{chicane}(E_b)$ for an energy scan.

The rotation angle $\theta = \arctan(-0.4374)$ equals to the angle of the straight line in Fig. 16. However, after normalization and comparison of $(x^{(4)}_{chicane}(E_b))_{rot}$ with x12Pos, no improvement for σ_{E_b}/E_b was found when compared with the values in the previous section. One reason could be the less precise resolution of the difference (y4Pos - y^4_{jitter}), which was found to be 3.2 μm compared to 2.3 μm (see Eq. (17) and Fig. 15). Furthermore, the value of $\theta = \arctan(-0.4374) = 23.49°$ cannot convincingly alone explain the difference between the two resolution values. Indeed, the amount of rotation needed to remove the difference is

$$\frac{\sigma_{E_b}}{E_b} = \frac{2.3\ \mu\mathrm{m}}{5\ \mathrm{mm}\cdot\cos\theta} = 8.5\cdot 10^{-4}$$
$$\rightarrow \theta = \arccos\left(\frac{2.3\ \mu\mathrm{m}}{5\ \mathrm{mm}\cdot 8.5\cdot 10^{-4}}\right) = 57°\ , \tag{20}$$

which is much too large when compared to the expectation of at most some degrees.

7 Summary

The beam energy resolution, σ_{E_b}/E_b, was measured by employing a 4-magnet chicane in End Station A at the Stanford Linear Accelerator Center. The chicane was commissioned in 2006/2007 for the experiment T474/491. The resolution σ_{E_b} is understood as the smallest variation of energy which can be measured in a reliable way by the spectrometer. Some imperfect readings of the NMR probes in the magnets, missing information on BPM alignment and, more important, the lack of a complementary or redundant method for absolute E_b measurements allowed only to perform relative beam energy determinations.

Due to large beam position jitters in the mid-chicane, a method was developed to subtract this jitter using data from BPMs outside the chicane. The method is in general based on the assumption that the jitter of interest can be written as a linear combination of X- and Y-positions as well as X- and Y-tilts from the BPMs upstream and downstream of the chicane.

In order to employ the BPMs downstream of the chicane it has to be ensured that the upstream beam path is fully restored downstream of the chicane. Unfortunately, this condition was not realized, probably caused by some non-demagnetization effects and different responses of the magnets using a common current. Such shortcomings are able to introduce a beam offset in the BPMs downstream, which is correlated with the beam energy. Thereby, these BPMs could not be used for beam jitter measurements and, as a consequence, some less precise beam energy resolution is obtained.

In summary, the beam energy resolution of the 4-magnet chicane, σ_{E_b}/E_b, has been measured as

$$\frac{\sigma_{x4Pos}^{MeV}}{E_b} = \frac{\sigma_{E_b}}{E_b} = \frac{24.3 \text{ MeV}}{28.5 \text{ GeV}} = 8.5 \cdot 10^{-4} \; . \tag{21}$$

This value is larger than the request of 10^{-4} (or better) for the ILC, but substantial improvements for future BPM-based spectrometers, as discussed in the note, indicate that the ILC goal can be achieved.

References

[1] J. Brau et al., International Linear Collider Reference Design Report, ILC-REPORT-2007-001.

[2] V.N. Duginov et al., LC-DET-2004-031.

[3] R. Assmann et al., Eur. Phys. J. C39 (2005) 253, CERN-PH-EP-2004-032 and CERN-AB-2004-030 OP.

[4] M. Slater et al., Nucl. Instr. Meth. A 592 (2008) 201.

[5] M. Hildreth et al., SLAC T-474, June 2004 and SLAC T-491, August 2006.

[6] R. Arnold et al., Proc. of PAC07, Albuquerque, New Mexico, 2007, USA.

[7] M. Viti, Thesis, submitted to Humboldt-Universität zu Berlin, DESY-THESIS-2010-007, February 2007.

[8] S. Kostromin and M. Viti, Magnetic Measurements for Magnets 10D37, ILC-SLACESA TN-2008-1, February 2008.

[9] E. Torrence et al., SLAC T-475, June 2004.

[10] J. Kent et al., SLAC-PUB-5110 (1990);
S. Herzbach, Proc. of the International Linear Collider Workshop, Batavia, Illinois, USA, October 2000.